Induced antiferromagnetism and large magnetoresistance in $RuSr_2(Nd,Y,Ce)_2Cu_2O_{10-\delta}$ ruthenocuprates

A. C. Mclaughlin*

Department of Chemistry, University of Aberdeen, Meston Walk, Aberdeen AB24 3UE, United Kingdom

F. Sher

Chemical and Materials Engineering Department, Pakistan Institute of Engineering and Applied Sciences, Nilore, Islamabad 45650, Pakistan

S. A. J. Kimber and J. P. Attfield

Centre for Science at Extreme Conditions and School of Chemistry, University of Edinburgh, King's Buildings, Mayfield Road, Edinburgh EH9 3JZ, United Kingdom

$RuSr_2(Nd,Y,Ce)_2Cu_2O_{10-\delta}$ ruthenocuprates have been studied by neutron diffraction, and magnetotransport and magnetization measurements, and the electronic phase diagram is reported. Separate Ru and Cu spin ordering transitions are observed, with spontaneous Cu antiferromagnetic order for low hole-doping levels p, and a distinct, induced-antiferromagnetic Cu spin phase in the $0.02 < p < 0.06$ pseudogap region. This ordering gives rise to large negative magnetoresistances which vary systematically with p in the $RuSr_2Nd_{1.8-x}Y_{0.2}Ce_xCu_2O_{10-\delta}$ series. A collapse of the magnetoresistance and magnetization in the presuperconducting region may signify the onset of superconducting fluctuations.

I. INTRODUCTION

In the past 20 years layered copper oxides such as $La_{2-x}Sr_xCuO_4$ (Ref. [1]) and $YBa_2Cu_3O_{6+x}$ (Ref. [2]) have been extensively studied due to the observation of high-temperature superconductivity (HTSC). A final theory of HTSC has yet to be established although there is increasing evidence that the pairing mechanism is mediated by magnetic excitations.[3,4] Recently a sharp magnetic excitation or resonance has been observed by neutron diffraction in both hole doped[4] and electron doped materials.[3] The resonance energy E_r scales with T_c so that $E_r \sim 5.8 k_B T_c$ for both hole and electron doped materials demonstrating that it is a fundamental property of the superconducting copper oxides. Another leading issue is the observation of a pseudogap below a characteristic temperature T^* in underdoped cuprates. It is still unclear whether the pseudogap represents a new electronic state which competes with the superconducting phase or if the pseudogap state represents a precursor to the superconducting d-wave gap[5,6] but further knowledge of this state may lead to greater insight of the superconductivity mechanism. Large bulk negative magnetoresistances ($MR = ((\rho_H - \rho_0)/\rho_0)$) have recently been observed in underdoped 1222 ruthenocuprates at low temperatures, up to $MR = -49\%$ at 4 K and 9 T in $Ru_{0.8}Ta_{0.2}Sr_2Nd_{0.95}Y_{0.15}Ce_{0.9}Cu_2O_{10}$,[7–10] demonstrating strong spin-charge coupling within the CuO_2 planes. Significant MR is observed over a wide hole-doping range ($0.01 \leq p \leq 0.06$)[8] and hence can be used to probe the electronic states in the pseudogap region.

Layered ruthenocuprate materials $RuSr_2RECu_2O_8$,[11,12] $RuSr_2(RE_{2-x}Ce_x)Cu_2O_{10-\delta}$ (Ref. [13]) (RE=Sm,Gd,Eu), and $Pb_2RuSr_2Cu_2O_8Cl$ (Ref. [14]) have been extensively studied due to the presence of coexisting weak ferro-

magnetism and superconductivity. Large $-MR$'s are observed in the new 1222-type ruthenocuprate series $RuSr_2Nd_{1.8-x}Y_{0.2}Ce_xCu_2O_{10-\delta}$ ($0.7 \leq \times \leq 0.95$) at low temperatures;[7,8] $-MR$ initially rises to $\sim 2\%$ below the Ru spin ordering temperature, T_{Ru}, as observed in other superconducting ruthenocuprates but increases dramatically on cooling. Neutron diffraction studies have shown that below T_{Ru}, additional peaks from a $\left(\frac{1}{2}\frac{1}{2}\frac{1}{2}\right)$ magnetic superstructure are observed, which can be fitted by a model of antiferromagnetically ordered Ru moments aligned in the c direction.[7] The Cu spins order antiferromagnetically in the ab plane with a $\left(\frac{1}{2}\frac{1}{2}0\right)$ superstructure below a second transition at T_{Cu}, as shown in Fig. 1. The variation of $-MR$ with temperature and field is characteristic of charge transport by magnetopolarons—small ferromagnetic regions surrounding each Cu hole within a matrix of antiferromagnetically ordered Cu^{2+} spins.[15] An applied magnetic field cants the Ru spins into a ferromagnetic arrangement, which induces partial ferromagnetism in the CuO_2 planes thereby increasing the mobility of the magnetopolarons, giving the observed, negative MR's.[8] Magnetopolaron hopping is a thermally activated process, leading to a characteristic exponential rise in $-MR$[16] below the Cu spin transition T_{Cu}.[7]

The magnetotransport in 1222 ruthenocuprates is also very sensitive to lattice effects. In a series of $RuSr_2R_{1.1}Ce_{0.9}Cu_2O_{10-\delta}$ (R=Nd, Sm, Eu, and Gd with Y) samples where the hole-doping level is constant, the high-field MR does not correlate with the paramagnetic moment of the R cations, but shows an unprecedented crossover from negative to positive MR values as $\langle r_A \rangle$, the mean A site ($R_{1.1}Ce_{0.9}$) cation radius, decreases.[8] This lattice effect is further evidenced from studies of $Ru_{1-x}Ta_xSr_2Nd_{0.95}Y_{0.15}Ce_{0.9}Cu_2O_{10}$ materials; $MR_{9\ T}(4\ K)$ increases from -28% to -49% as x increases from 0 to 0.2

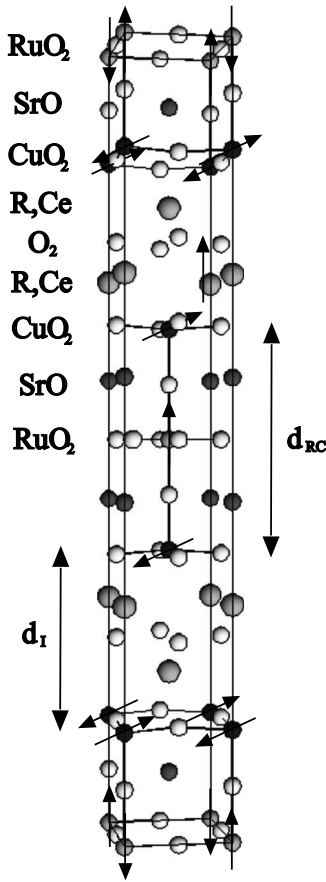FIG. 1. Crystal and magnetic structures of $RuSr_2Nd_{1.8-x}Ce_xY_{0.2}Cu_2O_{10-\delta}$. The interplanar separation of CuO_2 planes, d_I, and thickness of the $CuO_2 \cdot SrO \cdot RuO_2 \cdot SrO \cdot CuO_2$ ruthenium copper oxide slabs, d_{RC}, are labeled.

which further expands the unit cell.[10] The latter MR is the largest reported for ceramic copper oxide materials at this field strength and is comparable to values (at higher temperatures) in spin-polarized conductors such as the colossal magnetoresistant (CMR) manganites[17,18] and Sr_2FeMoO_6.[19]

In this paper, further results from a neutron diffraction, magnetoresistance and magnetic study of the ruthenocuprate series $RuSr_2Nd_{1.8-x}Y_{0.2}Ce_xCu_2O_{10-\delta}$ will be presented. The results demonstrate that the magnetic order in the RuO_2 planes induces long range antiferromagnetism in the CuO_2 plane across the pseudogap region, which results in the large magnetoresistances.

II. SAMPLE PREPARATION AND ANALYSIS

Samples of $RuSr_2Nd_{1.8-x}Y_{0.2}Ce_xCu_2O_{10-\delta}$ ($x=0.70, 0.75, 0.80, 0.85, 0.90, 0.95$) and $RuSr_2Nd_{1.0}Y_{0.1}Ce_{0.9}Cu_2O_{10-\delta}$ were prepared by the solid-state reaction of stoichiometric powders of Nd_2O_3, Y_2O_3, RuO_2, CuO, CeO_2, and $SrCO_3$, as described elsewhere.[8] Part of the "as prepared" $x=0.90$ and 0.95 samples were annealed for 24 h under flowing N_2 at 600 °C and furnace cooled to form more oxygen-deficient samples. Part of the as-prepared $x=0.70, 0.75,$ and 0.80, samples were annealed for 24 h un-

der flowing O_2 at 800 °C to reduce the oxygen deficiency δ.

Room temperature x-ray diffraction patterns were collected on a Bruker D8 Advance diffractometer with twin Gobel mirrors using Cu $K\alpha_1$ radiation. Data were collected over the range $5° < 2\theta < 100°$, with a step size of 0.02°. The profiles could all be indexed on a tetragonal $I4/mmm$ symmetry space group as previously reported for the 1222 ruthenocuprates;[20] a small amount of a secondary 1212 phase $RuSr_2(Nd, Y)Cu_2O_8$ is present in all samples.

The unit cell of $RuSr_2Nd_{1.8-x}Y_{0.2}Ce_xCu_2O_{10-\delta}$ consists of RuO_2, SrO, and CuO_2 layers stacked as in $RuSr_2GdCu_2O_8$, but in this case the CuO_2 layers are separated by a $Nd_{1.8-x}Ce_xY_{0.2}O_2$ block rather than a single rare earth layer. It has previously been reported that oxygen vacancies in $RuSr_2Gd_{2-x}Ce_xCu_2O_{10-\delta}$ are located on the O(4) sites within the $Gd_{2-x}Y_{0.2}Ce_xO_2$ block and that the concentration of oxygen vacancies increases as x decreases.[20] The oxygen contents of the present samples were determined by thermogravimetric analysis in a 5% H_2/N_2 atmosphere using a Stanton Redcroft 780 thermal analyzer. Data were recorded at a rate of 3 °C/min between temperatures of 20 and 800 °C. The samples decomposed to a mixture of Cu, Ru, SrO, CeO_2, Nd_2O_3 and Y_2O_3 in two steps between 300 and 750 °C, enabling δ to be determined from the mass loss. The results in Table I confirm that the oxygen deficiency decreases with Ce content in $RuSr_2Nd_{1.8-x}Y_{0.2}Ce_xCu_2O_{10-\delta}$ as x increases from 0.7 to 0.95, δ changes from 0.0905 to 0.015. Thermogravimetric analysis also shows that N_2 annealing increases δ, whereas annealing the samples under flowing O_2 results in a decrease in δ. X-ray appearance near-edge structure studies have shown that Ru remains in the formal +5 state in the 1222 ruthenocuprates (although this is not true of 1212 types), e.g., the measured Ru valence remains at 4.95(5) as x increases from 0.5 to 1.0 in $RuSr_2Gd_{2-x}Ce_xCu_2O_{10-\delta}$,[24] and so reliable Cu hole-doping concentrations p can be calculated from the cation and oxygen contents as $p = (1 - x - 2\delta)/2$, giving the values shown in Table I.

III. MAGNETIZATIONS

Magnetizations were measured between 5 and 300 K on a Quantum Design superconducting quantum interference device magnetometer in an applied field of 100 Oe after zero-field cooling (ZFC) and field cooling (FC), and data for representative $RuSr_2Nd_{1.8-x}Y_{0.2}Ce_xCu_2O_{10-\delta}$ samples are displayed in Fig. 2. Neutron diffraction (see later) shows that two magnetic transitions occur; canted antiferromagnetic (weak ferromagnetic) Ru spin ordering at T_{Ru} and antiferromagnetic order of the Cu spins at a lower-temperature transition T_{Cu}. A deviation between ZFC and FC data is evidenced for all samples. In the ZFC data M/H initially increases due to the weak ferromagnetic ordering of the Ru spins below T_{Ru} and at lower temperatures M/H is reduced as the Cu spins order antiferromagnetically. The irreversibility observed in ZFC and FC data arises due to a Dzyaloshinsky-Moriya (DM)[21,22] exchange between neighboring Ru sites, which is possible due to the tilts and rotations of the RuO_6 octahedra around c.[20] The field causes both

TABLE I. Variation of hole-doping level, p, and magnetoresistances, T_{Ru}, T_{Cu}, M_{max}, and δ, with x in the RuSr$_2$Nd$_{2.0-x-y}$Ce$_x$Y$_y$Cu$_2$O$_{10-\delta}$ solid solutions; $y=0.2$ in all samples except where otherwise indicated.

p	x	Anneal	δ	MR$_{7\ T}$ (5 K) (%)	T_{Ru} (K)	T_{Cu} (K)	M_{max} (emu mol^{-1})
0.010	0.95	N$_2$	0.015	−14	180	110	6.57
0.013	0.90	N$_2$	0.037	−17	180	115	7.98
0.017	0.90 ($y=0.1$)	Air	0.033	−29	165	104	5.47
0.021	0.95	Air	0.004	−20	150	77	6.00
0.033	0.90	Air	0.017	−22	130	59	7.39
0.042	0.85	Air	0.033	−23	117	49	4.73
0.046	0.80	Air	0.054	−22	95	41	3.02
0.052	0.75	Air	0.073	−21	85	33	1.32
0.055	0.80	O$_2$	0.045	−19	90	35	2.55
0.055	0.70	Air	0.095	−19	78	27	0.64
0.057	0.75	O$_2$	0.068	−17	78	29	0.85
0.059	0.70	O$_2$	0.091	−15	73	25	0.42

the Ru and Cu spins to cant out of their original direction and align a component of their moments with the direction of H.[7,23]

It has previously been shown that T_{Ru} can be determined by extrapolating the maximum $(-dM/dT)$ slope to zero magnetization, while T_{Cu} is estimated from the temperature of the maximum zero-field cooled magnetization (M_{max}).[7,8] These parameters are shown in Table I and the transition temperatures have been used to construct the phase diagram in Fig. 3. Both T_{Ru} and T_{Cu} decrease as the Cu hole-doping level p increases through changes in x and δ in our RuSr$_2$Nd$_{1.8-x}$Y$_{0.2}$Ce$_x$Cu$_2$O$_{10-\delta}$ samples. A similar decrease in T_{Ru}, from 110 to 50 K, is seen as x decreases from 1.0 to 0.5 in RuSr$_2$Gd$_{2-x}$Ce$_x$Cu$_2$O$_{10-\delta}$.[24] Furthermore, insertion of hydrogen into RuSr$_2$Eu$_{1.4}$Ce$_{0.6}$Cu$_2$O$_{10-\delta}$, which reduces the hole content, increases T_{Ru} from 92 to 167 K.[25] Although T_{Ru} decreases monotonically with doping in RuSr$_2$Nd$_{1.8-x}$Y$_{0.2}$Ce$_x$Cu$_2$O$_{10-\delta}$ (Fig. 2) T_{Cu} shows a discontinuity near $p=0.02$. This is the doping limit for long range antiferromagnetism in simple cuprates, and neutron diffraction shows that this is the boundary between normal (spontaneous) and induced-antiferromagnetic Cu spin phases (see later).

IV. MAGNETOTRANSPORT MEASUREMENTS

Magnetoresistance measurements were performed on sintered polycrystalline bars (approximate dimensions $4\times4\times12$ mm^3) between 4 and 290 K using a standard four-probe ac technique on a Quantum Design Physical Property Measurement System in magnetic fields up to 7 T. All of the RuSr$_2$Nd$_{1.8-x}$Y$_{0.2}$Ce$_x$Cu$_2$O$_{10-\delta}$ samples are semiconducting down to 4 K and do not show superconducting transitions or resistive anomalies at the magnetic transitions; representative plots are shown in Fig. 4.
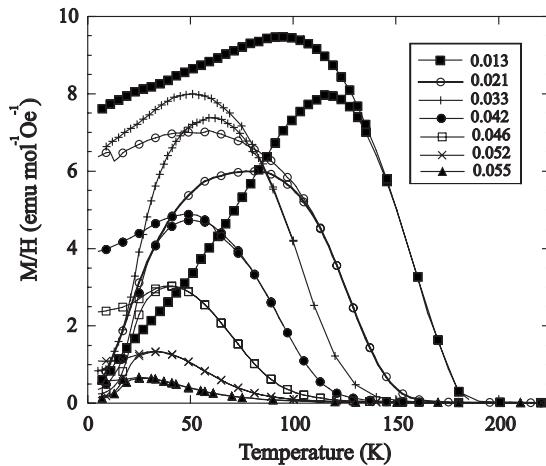

FIG. 2. Variable temperature magnetization data (zero field and field cooled) for the RuSr$_2$Nd$_{1.8-x}$Ce$_x$Y$_{0.2}$Cu$_2$O$_{10-\delta}$ solid solutions recorded in $H=100$ Oe.

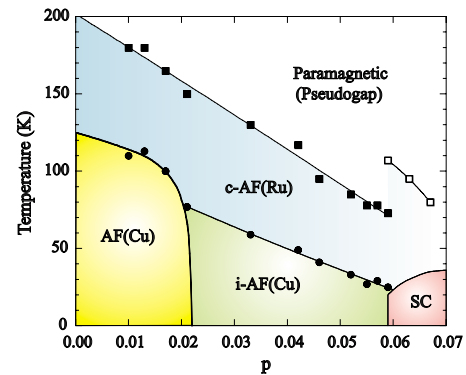
FIG. 3. (Color online) Electronic phase diagram for 1222-type ruthenocuprates. Ordering temperatures for the Ru spins (T_{Ru}, squares) and Cu spins (T_{Cu}, circles) at hole dopings $p<0.06$ are from RuSr$_2$Nd$_{1.8-x}$Y$_{0.2}$Ce$_x$Cu$_2$O$_{10-\delta}$ phases and RuSr$_2$NdY$_{0.1}$Ce$_{0.9}$Cu$_2$O$_{9.967}$ in this study. T_{Ru} (open squares) and superconducting critical temperatures (diamonds) for RuSr$_2$Gd$_{2-x}$Ce$_x$Cu$_2$O$_{10-\delta}$ ($x=0.6-0.8$) samples are shown in the $p=0.06-0.07$ region.
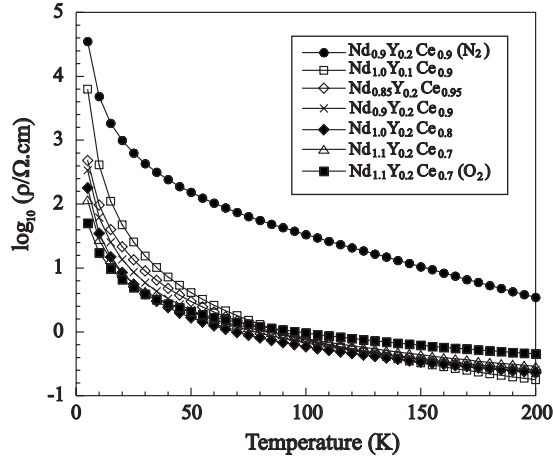
FIG. 4. Variation of the resistivity with temperature for representative $RuSr_2(Nd,Y,Ce)_2Cu_2O_{10-\delta}$ samples evidencing nonmetallic behavior.

The variation of MR with H for the $RuSr_2Nd_{1.8-x}Y_{0.2}Ce_xCu_2O_{10-\delta}$ samples is displayed in Fig. 5. Large negative magnetoresistances are observed at 5 K for all samples. Microstructural effects such as domain or grain boundary resistances are evident in the low field responses, as the MR-H curvature is negative for as-prepared samples but positive for O_2 and N_2-annealed materials. An increase in grain boundary resistances may also account for the anomalously high resistivity of the N_2-annealed $x=0.9$ sample (Fig. 4). However, the high-field MR's are linear and the high-field values (Table I and Fig. 6) show a strikingly smooth variation with the hole-doping level p, suggesting that intrinsic
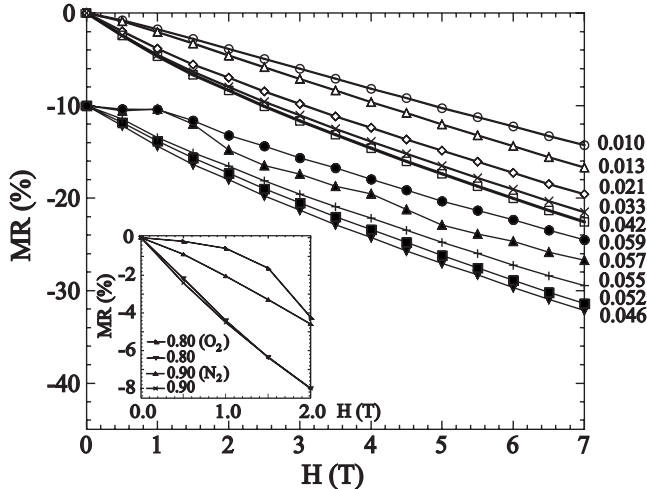

FIG. 5. Magnetoresistances MR_H ($=\rho(H)-\rho(0)/\rho(0)$) for sintered $RuSr_2Nd_{1.8-x}Y_{0.2}Ce_xCu_2O_{10-\delta}$ materials at 5 K in magnetic fields up to $H=7$ T. Doping values p are shown and data for $p > 0.044$ samples are offset by -10% MR for clarity. The inset shows the low-field MR for $x=0.8$ (as synthesized and annealed in O_2) and $x=0.9$ (as synthesized and annealed in N_2) which evidence microstructural effects such as domain or grain boundary resistances, as the MR-H curvature is negative for as-prepared samples but positive for O_2 and N_2-annealed materials.
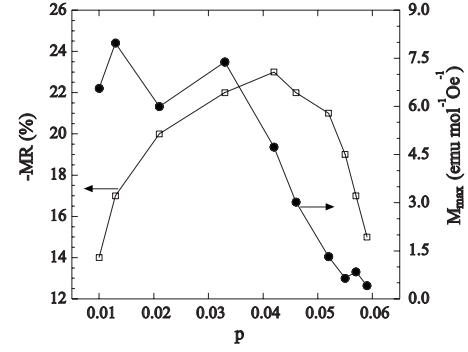

FIG. 6. Variations of the $-MR_{7\ T}(5\ K)$ magnetoresistance and the maximum value of magnetization (M_{max}) with hole doping p in the $RuSr_2Nd_{1.8-x}Y_{0.2}Ce_xCu_2O_{10-\delta}$ series.

factors dominate.[8] The initial rise of $-MR_{7\ T}(5\ K)$ for $p=0$ to 0.04 has been attributed to the increase in the number of holes acting as magnetopolaron carriers in the CuO_2 planes. The applied magnetic field cants the Ru and Cu spins toward a parallel alignment increasing the magnetopolaron mobility and resulting in large $-MR$. The peak in $-MR_{7\ T}(5\ K)$ at $p=0.04$ does not correspond to any discontinuity in T_{Ru} and T_{Cu} and so does not indicate a phase boundary, but is accompanied by the onset of a sharp decline of the maximum magnetization M_{max} at T_{Cu} above $p=0.033$, also shown in Fig. 6. This suggests that magnetopolarons in the CuO_2 planes are lost above $p=0.04$ due to the onset of d-wave pairing correlations between the Cu holes, eventually leading to superconductivity for $p > 0.06$. Thus the magnetoresistance is sensitive to the competition between antiferromagnetic and superconducting fluctuations in the induced antiferromagnetic (i-AF) phase.

V. NEUTRON DIFFRACTION

A. Structure refinements

Variable temperature neutron diffraction patterns of $RuSr_2Nd_{1.8-x}Y_{0.2}Ce_xCu_2O_{10}$ ($x=0.80$, 0.90, 0.95) and $RuSr_2Nd_{1.0}Y_{0.1}Ce_{0.9}Cu_2O_{10}$ for structure refinements were recorded at a wavelength of 1.5943 Å on instrument SuperD2B at the ILL, Grenoble. A 5 g sample was inserted into an 8 mm vanadium can and neutron diffraction patterns were recorded with an acquisition time of 1 h at 5, 30, 60, 90, 120, 150, 190, 220, and 290 K. Time of flight neutron diffraction data were recorded for the N_2-annealed sample of $RuSr_2Nd_{0.9}Y_{0.2}Ce_{0.9}Cu_2O_{10-\delta}$ on the high intensity instrument POLARIS at the ISIS Facility, Rutherford Appleton Laboratory. A 5 g sample was inserted into an 11 mm vanadium can and neutron diffraction patterns were recorded with an acquisition time of 1 h at 5, 30, 60, 100, and 140 K, (however, data collected at higher temperatures were unusable due to a technical problem).

The neutron diffraction patterns were all fitted by the Rietveld method[26] using the GSAS program.[27] The backgrounds were fitted using linear interpolation and the peak shapes were modeled using a pseudo-Voigt function. Excellent Rietveld fits were obtained (Fig. 7) for all profiles using a te-
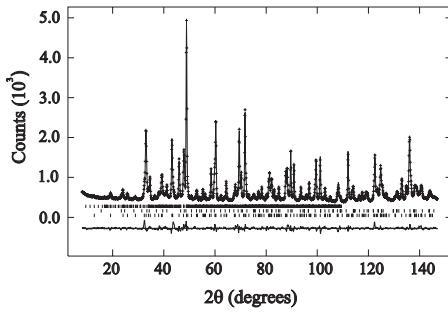
FIG. 7. Rietveld refinement fit to the 4 K SuperD2B neutron diffraction pattern of 1222-type $RuSr_2Nd_{0.85}Y_{0.2}Ce_{0.95}Cu_2O_{10-\delta}$. Lower, middle, and upper reflection markers correspond to $RuSr_2Nd_{0.85}Y_{0.2}Ce_{0.95}Cu_2O_{10-\delta}$, a trace of a secondary $RuSr_2(Nd,Y)Cu_2O_8$ phase, and magnetic 1222 phase reflections, respectively.

tragonal $I4/mmm$ structural model. There was no evidence of superstructure or orthorhombic distortion, but disordered rotations and tilts of the RuO_6 octahedra were evidenced as previously seen in $RuSr_2GdCu_2O_8$,[12] $Pb_2RuSr_2Cu_2O_8Cl$,[14] and $RuSr_2Gd_{1.5}Ce_{0.5}Cu_2O_{10-\delta}$.[20] These were modeled by splitting the oxygen sites of the RuO_6 octahedra. All of the metal occupancies refined to within ±1% of full occupancy and there was no evidence for cation antisite disorder. Variable temperature results for the $x=0.95$ sample are shown in Table II, and similar tables for the other samples have been deposited as auxiliary material.[28] Refined cell parameters and selected bond lengths at 5 K for all the samples studied are displayed in Table III.

The results summarized in Table III show that the 1222 structure does not change smoothly as a function of hole doping alone, but also varies with the Nd/Y/Ce and oxygen contents. Comparison of the three samples with Ce content $x=0.9$ shows that both an increasing oxygen deficiency δ (in the N_2-annealed sample) which removes holes, and the size effect of replacing some Y^{3+} by larger Nd^{3+} (compare N_2-annealed and $y=0.1$ samples, which have approximately constant δ) expand both the lattice parameters. Within the as-prepared $RuSr_2Nd_{1.8-x}Y_{0.2}Ce_xCu_2O_{10-\delta}$ series, as x decreases from 0.95 to 0.80, the size effect of replacing Ce^{4+} with larger Nd^{3+} counteracts the volume reduction due to increased hole doping, and no clear trend in a or cell volume emerges, although c contracts across the three samples. A small shift of the R cations away from the CuO_2 planes as the oxygen deficiency δ increases is evidenced by the variation of the $R-O(2)$ bond in Fig. 8. This is likely a consequence of stronger bonding between R cations and the remaining $O(4)$ atoms as vacancies are created in this layer.

The lattice parameters are plotted as a function of temperature in Fig. 9. A typical Debye-like thermal expansion of the lattice is observed for all samples and there is no evidence for the negative thermal expansion below T_{Ru} that was erroneously reported before.[7] Although no magnetostriction is seen in the lattice parameters, an anomaly is apparent when the contributions of the interplanar Cu-Cu distance d_I and the thickness of the ruthenocuprate slab d_{RC} to the c-axis length (Fig. 1) are considered. Figure 10 shows a clear

change in slope of d_I at T_{Ru} for three of the four samples, and in two cases d_I expands on cooling below T_{Ru}. By contrast, no anomalies are observed in the thermal variation of d_{RC}. A similar anomaly has previously been observed at the Ru spin ordering temperature from neutron diffraction measurements on $RuSr_2GdCu_2O_8$.[29] The change of slope for d_I does not correlate with the hole doping p, but does follow the oxygen deficiency δ, with the largest anomaly for the smallest δ (Figs. 8 and 10). The origin of this effect is unclear. The oxygen vacancies may frustrate the magnetic exchange interactions between RuO_2 layers, weakening the magnetostriction.

B. Magnetic diffraction

To observe weak magnetic diffraction peaks, variable temperature neutron diffraction patterns were recorded for $RuSr_2Nd_{1.0}Y_{0.1}Ce_{0.9}Cu_2O_{10-\delta}$ and $RuSr_2Nd_{0.9}Y_{0.2}Ce_{0.9}Cu_2O_{10-\delta}$ on the high intensity instrument D20 at the ILL at a wavelength of 2.4189 Å. A 5 g sample was inserted into an 8 mm vanadium can and the temperature was increased from 5 to 290 K at a rate of 1 K/min. Neutron diffraction data were recorded continuously and summed every 5 K. Neutron diffraction patterns were also recorded for $RuSr_2Nd_{1.0}Y_{0.2}Ce_{0.8}Cu_2O_{10-\delta}$ on D20 at temperatures 4, 10, 24, 40, 60, 80, 100, and 120 K.

We previously reported that the Ru spins order with a $\left(\frac{1}{2}\frac{1}{2}\frac{1}{2}\right)$ propagation vector and moments aligned parallel to the c direction in $RuSr_2Nd_{0.9}Y_{0.2}Ce_{0.9}Cu_2O_{10-\delta}$ below T_{Ru} $=130$ K.[7] As the temperature is decreased further the Cu spins order antiferromagnetically in the a-b plane with a $\left(\frac{1}{2}\frac{1}{2}0\right)$ superstructure (Fig. 1). The temperature variations of the magnetic superstructure intensities for this ($p=0.033$) phase and for $RuSr_2Nd_{1.0}Y_{0.2}Ce_{0.8}Cu_2O_{10-\delta}$ ($p=0.055$) are compared to those for the less doped ($p=0.017$) $RuSr_2Nd_{1.0}Y_{0.1}Ce_{0.9}Cu_2O_{10-\delta}$ in Fig. 11. The overlapped $\left[\left(\frac{1}{2}\frac{1}{2}\frac{1}{2}\right)+\left(\frac{1}{2}\frac{1}{2}0\right)\right]$ intensity and the $\left(\frac{1}{2}\frac{1}{2}2\right)$ peak intensity are sensitive to the magnitudes of the ordered Ru and Cu moments, respectively. The thermal evolutions of the $\left[\left(\frac{1}{2}\frac{1}{2}\frac{1}{2}\right)+\left(\frac{1}{2}\frac{1}{2}0\right)\right]$ intensities show that the Ru spin orderings are spontaneous in all three materials, with a sharp magnetic transition below which the intensities rapidly rise to a saturation value (taken to be the 4 K intensity, $I_{4 K}$). These data can be described by the critical expression $I/I_{4 K}=(1-T/T_c)^{2\beta}$; and fits in the $T_c/2<T<T_c$ regions give $\beta=0.35$, 0.26, and 0.25 for $p=0.017$, 0.033, and 0.055 samples, respectively. The value for the $p=0.017$ sample is typical of three-dimensional ordered antiferromagnets; however, the lower values for the $p=0.033$ and 0.055 samples suggest a more two-dimensional character. Two distinct behaviors for Cu spin order are revealed by the thermal variations of $I\left(\frac{1}{2}\frac{1}{2}2\right)$. Spontaneous Cu antiferromagnetism is observed for the $p=0.017$ sample, and the critical fit gives $\beta=0.38$ close to the value for Ru order.

The thermal evolutions of the $\left(\frac{1}{2}\frac{1}{2}2\right)$ intensity for both the $p=0.033$ and $p=0.055$ samples (Fig. 11) are different to that for $p=0.017$, as the intensity rises gradually below an ill-defined transition, and is not saturated down to 4 K. This is characteristic of an induced (nonspontaneous) magnetic order. The difference between the Cu spin orderings at doping

TABLE II. Refined atomic parameters for $RuSr_2Nd_{0.85}Ce_{0.95}Y_{0.2}Cu_2O_{10}$ (site occupancies; variable coordinates x, y, z and isotropic thermal parameters U) from variable temperature neutron diffraction data. Atom positions are Ru 2(a) (0, 0, 0), Sr 4(e) $(\frac{1}{2}, \frac{1}{2}, z)$, Nd/Ce/Y 4(e) $(\frac{1}{2}, \frac{1}{2}, z)$, Cu 4(e) (0, 0, z)), O(1) 16(n) $(x, 0, z)$, O(2) 8(g) $(0, \frac{1}{2}, z)$, O(3) 8(j) $(x, \frac{1}{2}, 0)$, and O(4) 4(d) $(0, \frac{1}{2}, \frac{1}{4})$. Refined cell parameters and selected bond lengths (Å) are also displayed.

Atom	Occupancy		Temperature (K)								
			5	30	60	90	120	150	190	220	290
Ru	1.00	U_{iso} (Å²)	0.0058(7)	0.0061(7)	0.0064(7)	0.0059(7)	0.0064(7)	0.0071(7)	0.0073(7)	0.0073(7)	0.0063(7)
Sr	1.00	z	0.07766(9)	0.07763(9)	0.07755(9)	0.07762(9)	0.07755(9)	0.07761(9)	0.07743(9)	0.07757(9)	0.07732(9)
		U_{iso} (Å²)	0.0095(5)	0.0099(5)	0.0106(5)	0.0109(5)	0.0114(5)	0.0120(5)	0.0134(5)	0.0134(5)	0.0149(5)
Nd/Ce/Y	1.00	z	0.20457(9)	0.20462(9)	0.20460(9)	0.20454(9)	0.20460(9)	0.20462(9)	0.20466(9)	0.20477(9)	0.20460(9)
		U_{iso} (Å²)	0.0037(5)	0.0038(5)	0.0040(5)	0.0039(5)	0.0051(5)	0.0044(5)	0.0054(5)	0.0055(5)	0.0065(5)
Cu	1.00	z	0.14364(8)	0.14367(8)	0.14360(8)	0.14373(8)	0.14375(8)	0.14372(8)	0.14373(8)	0.14370(8)	0.14372(8)
		U_{iso} (Å²)	0.0037(4)	0.0038(4)	0.0036(4)	0.0039(4)	0.0039(4)	0.0044(4)	0.0046(4)	0.0046(4)	0.0053(4)
O(1)	0.25	x	−0.028(4)	−0.033(4)	−0.036(4)	−0.036(4)	−0.041(4)	−0.041(4)	−0.043(4)	−0.046(4)	−0.046(4)
		z	0.0668(1)	0.0668(1)	0.0667(1)	0.0667(1)	0.0666(1)	0.0665(1)	0.0665(1)	0.0663(1)	0.0662(1)
		U_{iso} (Å²)	0.016(1)	0.014(1)	0.015(1)	0.014(1)	0.012(1)	0.013(1)	0.013(1)	0.012(1)	0.014(1)
O(2)	1.00	z	0.15012(6)	0.15013(6)	0.15017(6)	0.15010(6)	0.15013(6)	0.15012(6)	0.15011(6)	0.15006(6)	0.15014(6)
		U_{iso} (Å²)	0.0043(4)	0.0040(4)	0.0045(4)	0.0048(4)	0.0049(4)	0.0056(4)	0.0057(4)	0.0061(4)	0.0068(4)
O(3)	0.50	x	0.1300(8)	0.1309(8)	0.1304(8)	0.1307(8)	0.1299(8)	0.1298(8)	0.1292(8)	0.1299(8)	0.1272(8)
		U_{iso} (Å²)	0.015(1)	0.015(1)	0.015(1)	0.016(1)	0.016(1)	0.017(1)	0.017(1)	0.018(1)	0.019(1)
O(4)	1.00	U_{iso} (Å²)	0.0062(6)	0.0057(6)	0.0060(6)	0.0070(6)	0.0065(6)	0.0066(6)	0.0073(6)	0.0074(6)	0.0079(6)
		a (Å)	3.84365(4)	3.84369(3)	3.84404(3)	3.84462(3)	3.84541(3)	3.84636(3)	3.84771(3)	3.84878(3)	3.85147(3)
		c (Å)	28.4934(6)	28.4932(6)	28.4945(5)	28.4971(6)	28.5017(5)	28.5069(5)	28.5170(5)	28.5256(5)	28.5480(5)
		V (Å³)	420.951(10)	420.959(8)	421.054(8)	421.219(8)	421.461(8)	421.745(9)	422.191(9)	422.553(8)	423.476(8)
		χ^2	1.17	1.19	1.20	1.13	1.14	1.16	1.14	1.09	0.99
		R_{WP} (%)	4.24	4.27	4.30	4.17	4.19	4.21	4.17	4.08	3.82
		R_P (%)	3.09	3.19	3.18	3.07	3.12	3.15	3.12	3.04	2.79
		d_{RC}	8.185(5)	8.187(5)	8.183(5)	8.192(5)	8.194(5)	8.194(6)	8.198(6)	8.198(6)	8.206(6)
		d_I	6.062(3)	6.060(3)	6.064(3)	6.057(3)	6.057(3)	6.060(3)	6.061(3)	6.065(3)	6.069(3)
		Cu-O(1)	2.192(5)	2.195(5)	2.195(5)	2.201(5)	2.206(5)	2.207(4)	2.207(5)	2.214(5)	2.220(5)
		Cu-O(2)	1.9307(3)	1.9307(3)	1.9311(3)	1.9309(3)	1.9313(3)	1.9318(2)	1.9324(3)	1.9329(3)	1.9344(3)
		Ru-O(1)	1.906(4)	1.907(4)	1.906(4)	1.905(4)	1.903(4)	1.902(4)	1.905(4)	1.901(4)	1.898(4)
		Ru-O(3)	1.9858(10)	1.9866(10)	1.9863(10)	1.9869(10)	1.9866(10)	1.9869(10)	1.9870(10)	1.9882(10)	1.9871(10)
		Cu-O(2)-Cu	169.0(2)	169.1(2)	168.9(2)	169.2(2)	169.2(2)	169.2(2)	169.2(2)	169.2(2)	169.1(2)
		Ru-O(3)-Ru	150.8(2)	150.7(2)	150.8(2)	150.7(2)	150.9(2)	150.9(2)	151.0(2)	150.9(2)	151.4(2)

TABLE III. Refined cell parameters and selected bond lengths (Å) for the $RuSr_2Nd_{2.0-x-y}Ce_xY_yCu_2O_{10-\delta}$ solid solutions from neutron powder diffraction data recorded at 5 K; $y=0.2$ in all samples except where otherwise indicated.

p	0.013	0.017	0.021	0.033	0.046
x	0.90 (N_2)	0.90, $y=0.1$	0.95	0.90	0.80
δ	0.037	0.033	0.004	0.017	0.054
a (Å)	3.84519(3)	3.84742(4)	3.84365(4)	3.84304(4)	3.84561(4)
c (Å)	28.4906(5)	28.4936(5)	28.4934(6)	28.4881(5)	28.4821(6)
V (Å^3)	421.247(8)	421.782(9)	420.951(10)	420.740(10)	421.215(9)
χ^2	5.7	1.41	1.17	3.30	1.00
R_{WP} (%)	1.67	4.56	4.24	4.23	3.99
R_P (%)	3.44	3.38	3.09	3.37	3.23
d_{RC}	8.162(2)	8.167(5)	8.185(5)	8.168(5)	8.176(5)
d_I	6.083(2)	6.080(3)	6.062(3)	6.076(3)	6.065(3)
Cu-O(1)	2.170(3)	2.194(4)	2.192(5)	2.173(4)	2.191(5)
Cu-O(2)	1.9307(2)	1.9326(3)	1.9307(3)	1.9302(3)	1.9302(3)
Ru-O(1)	1.915(2)	1.905(3)	1.906(4)	1.918(3)	1.910(3)
Ru-O(3)	1.9815(6)	1.9876(8)	1.9858(10)	1.9827(8)	1.9820(10)
R-O(2)	2.475(2)	2.476(2)	2.470(2)	2.472(2)	2.484(2)
R-O(4)	2.325(2)	2.320(2)	2.317(2)	2.320(2)	2.317(2)
Cu-O(2)-Cu	169.5(1)	169.0(2)	169.0(2)	169.1(2)	170.0(3)
Ru-O(3)-Ru	152.0(3)	150.9(2)	150.8(2)	151.5(2)	151.9(2)

levels of $p=0.017$ and $p=0.033$ is consistent with the discontinuity in T_{Cu} from magnetization data seen at $p=0.021$ in Fig. 3, and confirms that this is the boundary between spontaneous and induced-antiferromagnetic phases, with long range $(\frac{1}{2}\frac{1}{2}0)$ Cu spin order in both cases. This demonstrates that the Ru spin order induces Cu spin order across the $0.02 \leq p \leq 0.06$ pseudogap region where long range Cu antiferromagnetism is not normally observed in cuprates.

VI. DISCUSSION

The 1222-type ruthenocuprates are difficult materials to prepare. Single crystals or epitaxial films have not been reported, and polycrystalline samples always contain traces of 1212 type or other secondary phases. The intrinsic chemistry of 1222 phases is also complex. The present study of

FIG. 8. Variations of the 290 K R−O(2) bond length and the change in slope of d_I at T_{Ru} with δ in the $RuSr_2Nd_{2-x-y}Y_yCe_xCu_2O_{10-\delta}$ solid solutions.

$RuSr_2Nd_{1.8-x}Y_{0.2}Ce_xCu_2O_{10-\delta}$ demonstrates that both the R^{3+}/Ce^{4+} ratio and the deficiency of oxygen in the $(R,Ce)_2O_{2-\delta}$ block are important in controlling the hole doping p of the CuO_2 planes. The clear trends of magnetic transition temperatures (Fig. 3) and magnetoresistances (Fig. 6) with the experimentally determined p values show that these are meaningful, and that it is important to take oxygen deficiency into account when considering physical trends in 1222 materials.

Neutron diffraction (Fig. 11) shows that both the Ru and Cu spins order at distinct transitions. While the variable temperature neutron experiments provide direct measurements of T_{Ru} and T_{Cu}, useful estimates of the transition temperatures can be derived from the low-field magnetization measurements (Fig. 2), at least for comparative purposes. By combining these values with those of a superconducting $RuSr_2Nd_{1.4}Ce_{0.6}Cu_2O_{10-\delta}$ sample[30] and the $RuSr_2Gd_{2-x}Ce_xCu_2O_{10-\delta}$ system[31] which overlaps the superconducting regime, the composite electronic phase diagram for ruthenocuprates shown in Fig. 3 is constructed. T_{Ru} decreases with increased hole doping of the CuO_2 planes, but the discontinuity between the Nd- and Gd-based series at $p=0.06$ shows that R-cation size effects are also important. The magnetic coupling between RuO_2 layers becomes stronger as the thickness of the $(R,Ce)_2O_{2-\delta}$ block (Fig. 1) is decreased on changing from larger Nd^{3+} to smaller Gd^{3+}. The importance of Ru-Ru coupling through the $(R,Ce)_2O_{2-\delta}$ block is corroborated by the structural anomaly in d_I at T_{Ru} (Fig. 10) which is sensitive to the oxygen deficiency δ. Furthermore $RuSr_2Nd_{1.8-x}Y_{0.2}Ce_xCu_2O_{10-\delta}$ samples with $x=0.8$ (O_2 annealed) and $x=0.7$ (as prepared), which have the same hole concentration, $p=0.055$, but distinct values of δ (Table

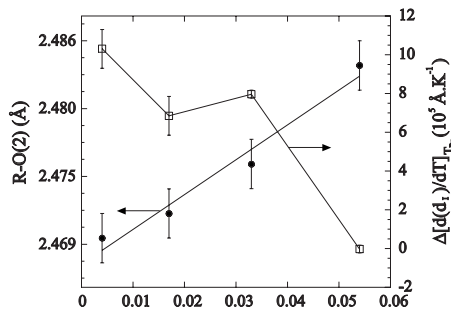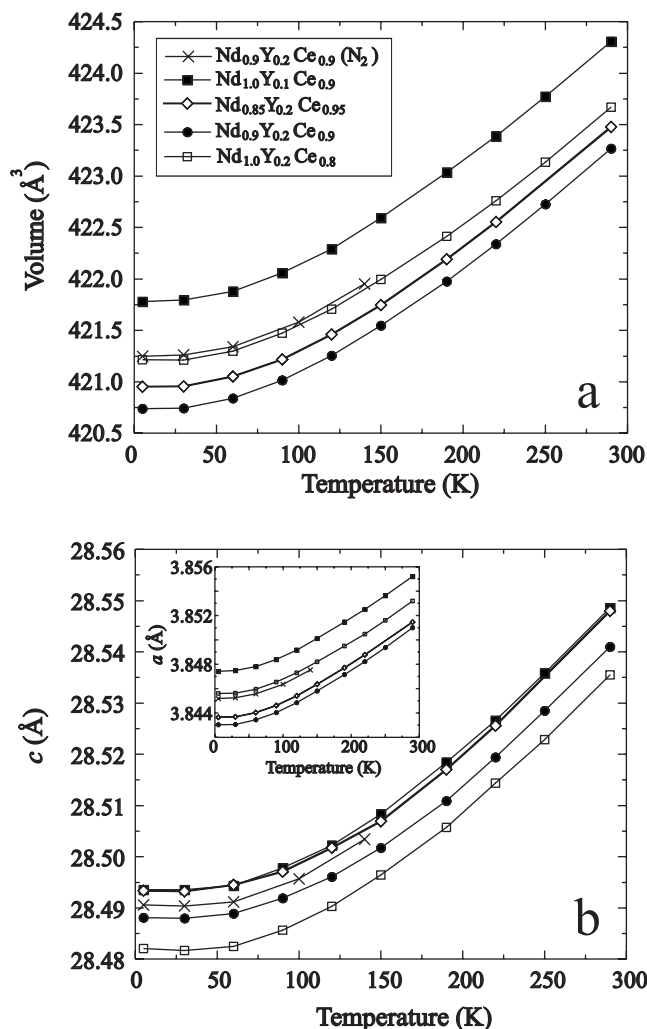FIG. 9. Temperature variations of (a) unit-cell volume and (b) lattice parameters c and a (inset) for representative $RuSr_2(Nd, Y, Ce)_2Cu_2O_{10-\delta}$ samples.

FIG. 10. Temperature variations of the interplanar CuO_2 separation, d_I, and the thickness of the ruthenocuprate slabs, d_{RC} (as defined on Fig. 1), in (a) $RuSr_2Nd_{1.0}Y_{0.1}Ce_{0.9}Cu_2O_{10-\delta}$ ($p=0.017$, $\delta=0.033$), (b) $RuSr_2Nd_{0.85}Y_{0.2}Ce_{0.95}Cu_2O_{10-\delta}$ ($p=0.021$, $\delta=0.004$), (c) $RuSr_2Nd_{0.9}Y_{0.2}Ce_{0.9}Cu_2O_{10-\delta}$ ($p=0.033$, $\delta=0.017$), and (d) $RuSr_2Nd_{1.0}Y_{0.2}Ce_{0.8}Cu_2O_{10-\delta}$ ($p=0.046$, $\delta=0.054$).

tiferromagnetism to superconducting transition. The induced nature of the Cu antiferromagnetism from $0.02 < p < 0.06$ is further corroborated by variable temperature neutron diffraction measurements on a sample in the AF region ($p=0.017$) and two samples in the i-AF region of the phase diagram with $p=0.033$ and $p=0.055$ (Fig. 11). The thermal evolution of the $\left(\frac{1}{2}\frac{1}{2}2\right)$ magnetic intensity for samples with $p < 0.02$ can be described by a critical expression. In contrast the intensity of the $\left(\frac{1}{2}\frac{1}{2}2\right)$ peak for samples with $p > 0.02$ increases gradually with decreasing temperature and there is no evidence of

I) exhibit significant differences in the magnetic parameters T_{Ru}, T_{Cu}, and M_{max} so that T_{Ru} decreases from 90 to 78 K as δ increases from 0.045 to 0.095 (Table I). Hence the magnetic transition temperatures T_{Ru} and T_{Cu} are dependent both on the hole concentration, p, and on the oxygen deficiency in the $(R, Ce)_2O_{2-\delta}$ block.

Figure 3 shows that coupling between the Ru and Cu spins in the low doped ruthenocuprates extends the limit of long range antiferromagnetic Cu spin order up to the border of superconductivity at 6% hole doping. The $p=0.02$ discontinuity in T_{Cu} marks the boundary between the spontaneous antiferromagnetic phase that is generic to cuprates, and an induced-Cu antiferromagnetic phase in the $0.02 < p < 0.06$ region where a "mixed" phase without long range magnetism is usually observed. This shows that the near-antiferromagnetic Ru spin order aligns the locally correlated Cu antiferromagnetic regions intrinsic to the mixed phase. We deduce that a direct boundary between induced-Cu antiferromagnetism and superconducting phases is present near $p \approx 0.06$. It will be useful to prepare further 1222 series that span this boundary to study directly the low-temperature an-
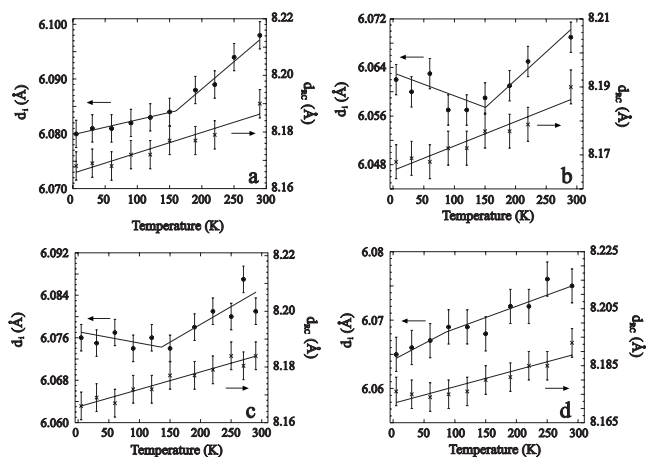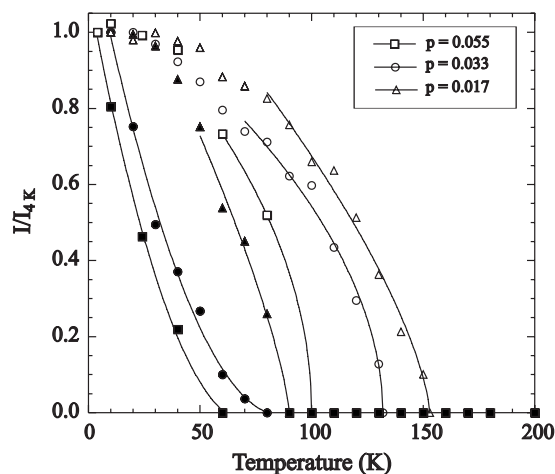

FIG. 11. Temperature variations of the integrated $\frac{1}{2}\frac{1}{2}2$ (bold symbols) and composite $\frac{1}{2}\frac{1}{2}0)+\left(\frac{1}{2}\frac{1}{2}\frac{1}{2}\right)$ (open symbols) magnetic diffraction peak intensities (relative to 4 K values) for $RuSr_2NdY_{0.1}Ce_{0.9}Cu_2O_{9.967}$ ($p=0.017$), $RuSr_2Nd_{0.9}Y_{0.2}Ce_{0.9}Cu_2O_{9.983}$ ($p=0.033$), and $RuSr_2Nd_{1.0}Y_{0.2}Ce_{0.8}Cu_2O_{9.955}$ ($p=0.055$) showing the Ru and Cu spin ordering transitions. Critical law fits in the range $T_c/2 < T < T_c$ are shown except for the $p=0.033$ and $p=0.055$, and $I\left(\frac{1}{2}\frac{1}{2}2\right)$ data which are fitted by an arbitrary curve.

saturation down to the lowest temperature recorded, which is characteristic of induced magnetic order.

Structural studies of $RuSr_2Nd_{1.8-x}Y_{0.2}Ce_xCu_2O_{10-\delta}$ by neutron diffraction show that a magnetostriction in the interplanar CuO_2 separation, d_I is observed at T_{Ru} so that there is a clear change in slope of d_I at T_{Ru} for three of the four samples (Figs. 8 and 10). A similar anomaly has previously been observed at the Ru spin ordering temperature from neutron diffraction measurements on superconducting $RuSr_2GdCu_2O_8$ (Ref. 29); the origin of this magnetostriction is not yet known. However, it has been demonstrated that the Ru spin ordering induces antiferromagnetic order in the CuO_2 plane from $p = 0.02$ to 0.059 and hence the magnetostriction in d_I could be a consequence of induced magnetic clusters within the CuO_2 plane at T_{Ru} which grow in size with decreasing temperature so that antiferromagnetic order is detected by neutron diffraction at lower temperatures. μSR experiments are under way to investigate this further.

Large negative magnetoresistances have previously been observed in lightly doped cuprates[32–34] as Cu spin reorientation of the antiferromagnetic phase in an applied field enhances the conductivity, particularly the c-axis transport. Results show that there is no significant variation in the MR upon increasing the oxygen deficiency, δ (Table I). This is clearly demonstrated by the magnetotransport properties of samples with $x = 0.8$ (O_2 annealed) and $x = 0.7$ (as prepared) which have the same hole concentration ($p = 0.055$) but significant differences in oxygen deficiency; $MR_{7\ T}(5\ K) = -19\%$ for both samples. Ru spin order in the ruthenocuprates extends Cu antiferromagnetism to higher dopings, enabling the trend of high-field MR with p (Fig. 6) to be discovered. As p increases to 0.042 in $RuSr_2Nd_{1.8-x}Y_{0.2}Ce_{0.9}Cu_2O_{10-\delta}$ a maximum in $-MR$ is evidenced; at the same time a sharp decline of the maximum magnetization M_{max} at T_{Cu} is observed, which is consistent with the loss of magnetopolarons in the CuO_2 planes. This suggests that both the spin-polarized antiferromagnetic and superconducting precursor phases are present in underdoped ruthenocuprates but the superconducting precursor phase is increasingly stabilized above $p = 0.042$ so that $-MR_{7\ T}(5\ K)$ and M_{max} fall rapidly as a result of the onset of d-wave pairing correlations between Cu holes, eventually leading to superconductivity for $p > 0.06$. Hence the magnetoresistance is sensitive to the competition between antiferromagnetic and superconducting fluctuations in the i-AF phase and could be used to probe the pseudogap state further.

VII. CONCLUSIONS

These results show that the physical properties of the underdoped $RuSr_2(Nd,Y,Ce)_2Cu_2O_{10-\delta}$ ruthenocuprates are dependent on both the $(Nd,Y)^{3+}/Ce^{4+}$ ratio and the oxygen deficiency within the $(Nd,Y,Ce)_2O_{2-\delta}$ block. A full chemical characterization of samples is therefore important in order to understand the complex physics of the 1222 ruthenocuprates, in which high-T_C superconductivity and large magnetoresistances can emerge from the interactions between weakly ferromagnetic RuO_2 layers and doped antiferromagnetic CuO_2 planes. Induced-antiferromagnetic $(1/2\ 1/2\ 0)$ Cu spin order is observed across the pseudogap region up to the onset of superconductivity, and the high-field MR varies systematically with Cu hole doping in the $RuSr_2Nd_{1.8-x}Y_{0.2}Ce_xCu_2O_{10-\delta}$ series. A collapse of $-MR$ and magnetization above $p = 0.042$ reveals the onset of d-wave spin pairing in the presuperconducting region. Further research will be needed to investigate whether phase segregation occurs in the presuperconducting region and to study the low-temperature antiferromagnetic to superconducting transition at $p > 0.059$.

*Author to whom correspondence should be addressed; a.c.mclaughlin@abdn.ac.uk

[1] J. G. Bednorz and K. A. Muller, Z. Phys. B: Condens. Matter **64**, 189 (1986).

[2] M. K. Wu, J. R. Ashburn, C. J. Torng, P. H. Hor, R. L. Meng, L. Gao, Z. J. Huang, Y. Q. Wang, and C. W. Chu, Phys. Rev. Lett. **58**, 908 (1987).

[3] S. D. Wilson, P. Dai, S. Li, S. Chi, H. J. Kang, and J. W. Lynn, Nature (London) **442**, 59 (2006).

[4] S. M. Hayden, H. A. Mook, P. Dai, T. G. Perring, and F. Dogan, Nature (London) **429**, 531 (2004).

[5] V. J. Emery and S. A. Kivelson, Nature (London) **374**, 434 (1995).

[6] A. Kanigel, M. R. Norman, M. Randeria, U. Chatterjee, S. Souma, A. Kaminski, H. M. Fretwell, S. Rosenkranz, M. Shi, T. Sato, T. Takahashi, Z. Z. Li, H. Raffy, K. Kadowaki, D. Hinks, L. Ozyuzer, and J. C. Campuzano, Nat. Phys. **2**, 447 (2006).

[7] A. C. Mclaughlin, F. Sher, and J. P. Attfield, Nature (London) **436**, 829 (2005); **437**, 1057 (2005).

[8] A. C. Mclaughlin, L. Begg, C. Harrow, S. A. J. Kimber, F. Sher, and J. P. Attfield, J. Am. Chem. Soc. **128**, 12364 (2006).

[9] V. P. S. Awana, M. A. Ansari, A. Gupta, R. B. Saxena, H. Kishan, D. Buddhikot, and S. K. Malik, Phys. Rev. B **70**, 104520 (2004).

[10] A. C. Mclaughlin, L. Begg, A. J. McCue, and J. P. Attfield, Chem. Commun. (Cambridge) **2007**, 2273.

[11] C. Bernhard, J. L. Tallon, C. Niedermayer, T. Blasius, A. Golnik, E. Brucher, R. K. Kremer, D. R. Noakes, C. E. Stronach, and E. J. Ansaldo, Phys. Rev. B **59**, 14099 (1999).

[12] A. C. McLaughlin, W. Zhou, J. P. Attfield, A. N. Fitch, and J. L. Tallon, Phys. Rev. B **60**, 7512 (1999).

[13] I. Felner, U. Asaf, Y. Levi, and O. Millo, Phys. Rev. B **55**, R3374 (1997).

[14] A. C. Mclaughlin, J. A. McAllister, L. D. Stout, and J. P. Attfield,

Phys. Rev. B **65**, 172506 (2002).

[15] E. L. Nagaev, JETP Lett. **6**, 18 (1967).

[16] P. Majumdar and P. Littlewood, Phys. Rev. Lett. **81**, 1314 (1998).

[17] *Colossal Magnetoresistance, Charge Ordering and Related Properties of Manganese Oxides*, edited by C. N. R. Rao and B. Raveau (World Scientific, Singapore, 1998).

[18] *Colossal Magnetoresistive Oxides*, edited by Y. Tokura (Gordon and Breach, New York, 2000).

[19] K. L. Kobayashi, T. Kimura, H. Sawada, K. Terakuraand, and Y. Tokura, Nature (London) **395**, 677 (1998).

[20] A. C. Mclaughlin, J. P. Attfield, U. Asaf, and I. Felner, Phys. Rev. B **68**, 014503 (2003).

[21] I. Dzyaloshinksy, Sov. Phys. JETP **5**, 1259 (1957).

[22] T. Moriya, Phys. Rev. **120**, 91 (1960).

[23] A. C. Mclaughlin and J. P. Attfield, J. Magn. Magn. Mater. **310**, 1961 (2007).

[24] G. V. M. Williams, L.-Y. Jang, and R. S. Liu, Phys. Rev. B **65**, 064508 (2002).

[25] I. Felner, U. Asaf, S. D. Goren, and C. Korn, Phys. Rev. B **57**, 550 (1998).

[26] H. M. Rietveld, Acta Crystallogr. **22**, 151 (1967).

[27] A. C. Larson and R. B. Von Dreele, General Structure Analysis System (GSAS), Report No. LAUR-86-748, Los Alamos National Laboratory, 1994 (unpublished).

[28] See EPAPS Document No. E-PRBMDO-76-054733 for further variable temperature crystallographic data. For more information on EPAPS, see http://www.aip.org/pubservs/epaps.html.

[29] O. Chmaissem, J. D. Jorgensen, H. Shaked, P. Dollar, and J. L. Tallon, Phys. Rev. B **61**, 6401 (2000).

[30] G. M. Kuz'micheva, A. I. Kurbakov, I. E. Kostyleva, A. S. Andreenko, and Yu. V. Esaulova, Physica C **349**, 149 (2004).

[31] G. V. M. Williams and M. Ryan, Phys. Rev. B **64**, 094515 (2001); p values were estimated by assuming equivalent hole concentration for $RuSr_2Nd_{1.4}Ce_{0.6}Cu_2O_{10-\delta}$ (oxygen annealed) and $RuSr_2Nd_{1.2}Y_{0.2}Ce_{0.6}Cu_2O_{10-\delta}$ (oxygen annealed) materials. The hole-doping level of the $RuSr_2Gd_{2-x}Ce_xCu_2O_{10-\delta}$ solid solutions could then be inferred by comparing T_c's of Nd and Gd analogs and assuming a constant increase in δ as x decreases as determined from $RuSr_2Nd_{1.8-x}Y_{0.2}Ce_xCu_2O_{10-\delta}$ (oxygen annealed) samples of known oxygen content.

[32] Y. Ando, A. N. Lavrov, and S. Komiya, Phys. Rev. Lett. **90**, 247003 (2003).

[33] A. N. Lavrov, H. J. Kang, Y. Kurita, T. Suzuki, S. Komiya, J. W. Lynn, S.-H. Lee, P. Dai, and Y. Ando, Phys. Rev. Lett. **92**, 227003 (2004).

[34] T. Thio, T. R. Thurston, N. W. Preyer, P. J. Picone, M. A. Kastner, H. P. Jenssen, D. R. Gabbe, C. Y. Chen, R. J. Birgeneau, and A. Aharony, Phys. Rev. B **38**, 905 (1988).